Final Report of the UGC Project entitled "Morphology tuning of nano gold using highly surface active inorganic molecules"

1. Physiochemical aspects of tetronics and surfactants for the synthesis of gold nanoparticles at different temperature and pH

Aqueous mixtures (total 10 ml) of tetronic (T904 (EO = 15, PO = 17) average molar mass = 6700, T908 (EO = 114, PO = 21) average molar mass = 25 000, and T1307 (EO = 72, PO = 32) average molar mass = 18 000) and $HAuCl_4$ were taken in screw-capped glass bottles with final concentrations of 10 mM and 0.5 mM, respectively. After mixing the components at room temperature, the reaction mixtures were kept in a water thermostat bath (Julabo F25) at a precise temperature of 70°C for six hours under static conditions. The color of the solution changed from colourless to pink-purple or purple with the passage of time and remained same thereafter in most of the cases. After six hours, the samples were cooled to room temperature and kept overnight. They were purified from pure water in order to remove unreacted tetronic. These samples were used for TEM analysis. In order to understand the reaction kinetics of the synthesis of gold nanoparticles (AuNPs), each reaction was monitored by simultaneous UV-visible measurements with temperature in the range of 20–70°C to determine the influence of micelle transitions on the synthesis of AuNPs. All reactions were performed in the UV cuvette with the help of a double beam UV-Vis spectrophotometer. This instrument is equipped with a TCC 240A thermo- electrically temperature controlled Cell Holder that allows measurement of the spectrum at a constant temperature within 1°C.

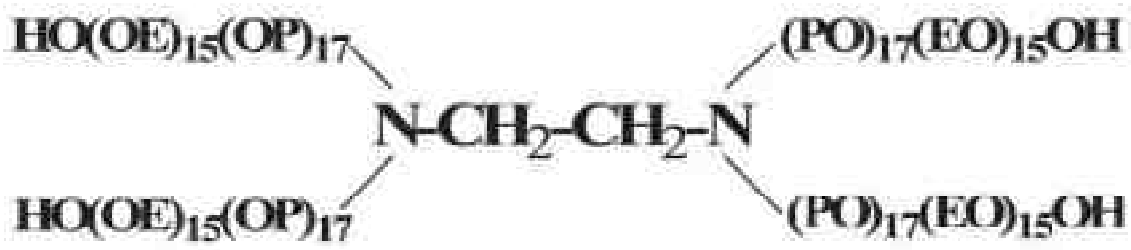

Figure 1: Structure of star shaped T904

Results and Discussion

Synthesis of Au NPs under temperature and pH effects

A typical UV-visible scan of an aqueous mixture of tetronic T904 with gold salt under the effect of temperature variation at pH = 6 without the use of any additional reducing or stabilizing agent is shown in Fig 2a. An absorbance at 540 nm due to the surface plasmon resonance (SPR) of AuNPs appears at around 34°C, which becomes prominent with the rise in temperature. Similar scans are obtained when the same reaction is carried out at other pH values, and with T908 and T1307 instead of T904. The variation in the intensity of 540 nm absorbance is depicted in Fig. 2b. Each plot shows a sigmoidal variation where the intensity of this peak remains insignificant over a certain temperature range, and then it instantaneously increases with the increase in temperature before tending to a constant value. It shows that the synthesis of AuNPs occurs only at a certain temperature which is known as the nucleation temperature (N_T, indicated by arrows in Fig. 2b); thereafter, an instant growth in the NPs causes an instant increase in the intensity. It levels off when the growth reaches a limiting value. The N_T values for T904, T908, and T1307 at different pH

values except at pH = 2 (where solution remains colourless and no synthesis of AuNPs is observed) are plotted in Fig. 2c. N_T decreases non-linearly with the increase in pH with relatively greater value for T904 followed by T1307 and T908. In other words, low pH induces the synthesis of Au NPs at high temperature and vice versa. Interestingly, N_T values from the three curves merge at pH = 12 irrespective of the nature of tetronics at 20°C which means that strongly basic medium facilitates the instantaneous reduction of Au(III) into Au(0).

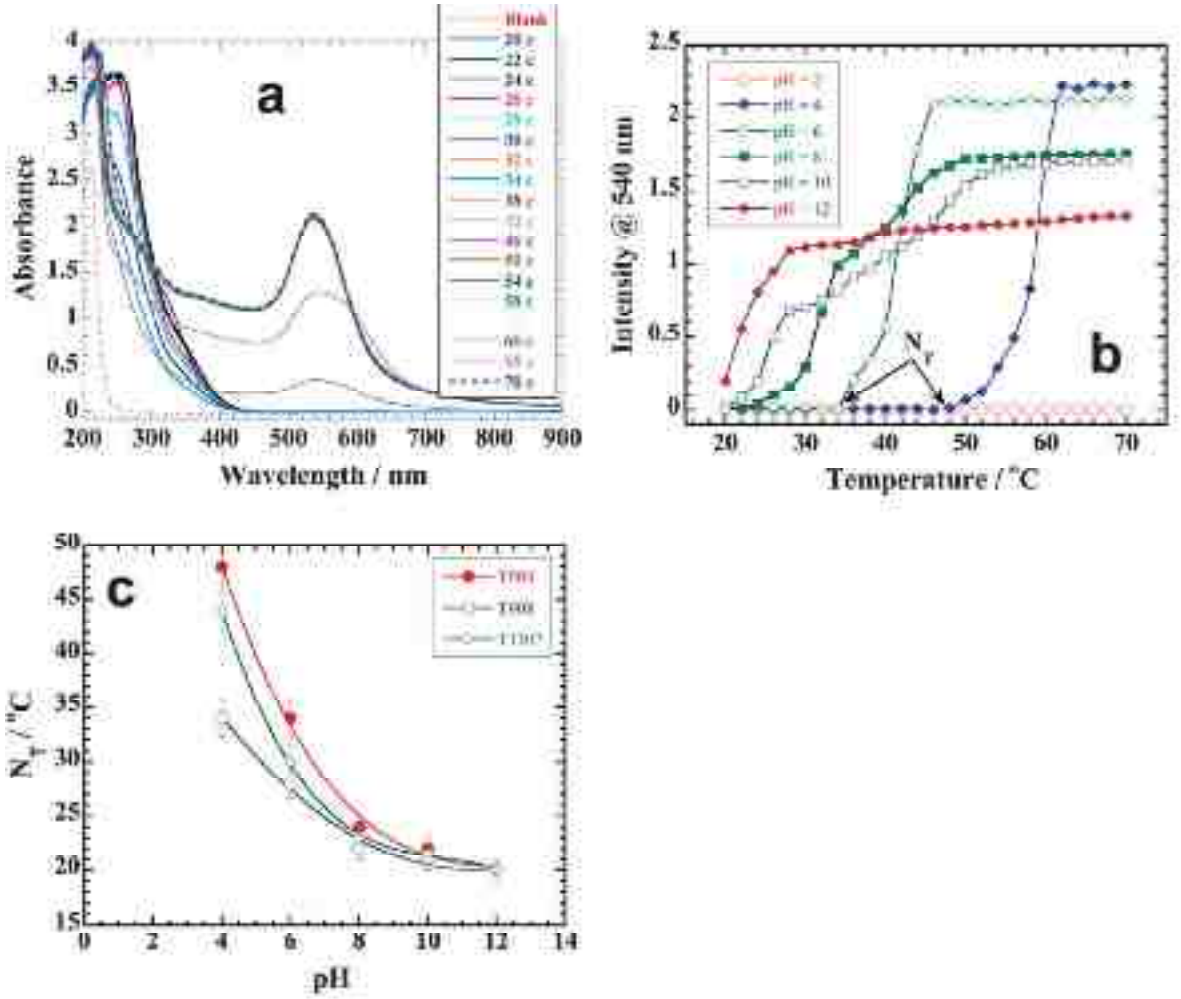

Figure 2(a) A typical example of a reaction in aqueous phase of 10 mM T904 with 0.5 mM HAuCl4 at pH = 6 under the effect of temperature variation from 20–70°C and simultaneously monitored by the UV-Visible measurements. Red dotted line refers to blank (i.e. aqueous 10 mM T904 without gold salt) and blue dotted line represents the scan at 70°C. Scans from bottom to top follow the 20–70°C temperature range. (b) Shows the variation of intensity of 540 nm peak versus temperature for the same reaction at different pH. N_T represents the nucleation temperature from where the synthesis of gold nucleating centres starts. (c) Plot of N_T versus pH for the reactions of different tetronics

Time effect

We have seen a pronounced pH effect on the micellization temperature of tetronics which consequently directly controls the nucleation temperature of AuNPs. Next, we have studied the effect of reaction time at a constant temperature of 70°C on the synthesis of AuNPs at different pH

values. Fig. 3a shows such a reaction at pH = 2 with a very weak absorbance at 540 nm of Au NPs in contrast to Figure 2b where we do not see this absorbance under the effect of temperature variation from 20 to 70°C. It means that the synthesis of AuNPs at pH = 2 is only noticed when the reaction is conducted at 70°C and that too for a much longer duration of time. On the other hand, this reaction also shows a prominent absorbance at 320 nm due to ligand to metal charge transfer complex (LMCT) between the charge donating sites of T904 (either oxygens or amine groups) and the electropositive centre of $AuCl_4^-$ ions. Note that the intensity of the 320 nm peak is absent in the blank run (i.e. in the absence of gold salt) and is maximum (at 1 minute of the reaction or) as soon as gold salt is added. Thereafter, it decreases with the passage of time because of the conversion of LMCT into nucleating centres upon the reduction of Au(III) into Au(0). Interestingly, we do not see the 320 nm peak for the reactions at pH = 8–12 which suggests the nonexistence of the LMCT complex in these reactions, and that is why N_T in Fig. 2c within this pH range is quite low in comparison to the reactions conducted at low pH values. A variation in the absorbance of 540 nm for all reactions of Fig. 2b under the effect of reaction time at 70°C have been depicted in Fig. 3b, where T904 is already in the micellized form and hence each plot only demonstrates the growth kinetics of AuNPs at different pH values. Each reaction shows that the absorbance of AuNPs increases instantaneously at a certain reaction time (indicated by arrows for some of the reactions), which we call as nucleation time (N_{time}), and its variation with pH is illustrated in Fig. 3c. At pH = 2, it takes 60 minutes to initiate the nucleation; thereafter, N_{time} rapidly decreases with the increase in pH while the nucleation starts within 1 minute of the start of the reaction for pH = 8–12. The results can be properly understood on the basis of LMCT formation. At pH = 2, a clear LMCT formation takes place at 320 nm (Fig. 3a) which exists till 60 minutes of the reaction and its variation is shown in Fig. 3d, whereas at pH = 4, it is very short lived and vanished within 5 minutes of the reaction. We do not see any peak at 320 nm for the reactions at higher pH values. Disappearance of the LMCT complex coincides with the appearance of AuNPs absorbance at 540 nm (indicated by arrows in Fig. 3d) which means that the N_{time} is the reaction time where the LMCT complex entirely converts into tiny nucleating centres to initiate the growth of Au NPs (Fig. 3b). Thus, LMCT formation is only related to the reaction pH. When the pH is low, amine groups are protonated, and LMCT formation takes place mainly due to the charge donation from predominantly ligand 3e u (p) electron rich ether oxygens of Polyethlene oxide (PEO) or Polypropylene Oxide (PPO) blocks to electron deficient metal 3b 1g (s*) molecular orbitals of $AuCl_4^-$ ions. On the other hand, at high pH, amine groups along with ether oxygens instantaneously reduce Au(III) into Au(0) and hence no LMCT complex forms. Thus, reduction potential of T904 is high when amine groups also participate in the reduction process along with ether oxygens and it is only possible in basic medium. That is why, N_{time} is less than 1 minute in basic medium while its value depends on the pH in acidic medium (Fig. 3c). Because pH = 4 is not expected to induce maximum protonation of amine groups and hence it takes about 5 minutes to initiate the nucleation in comparison to pH = 2, which consumes 60 minutes (Fig. 3c and d). That is why pH = 2 does not allow us to determine the N_T for the same reaction in Fig. 2b because of EO units than PO, therefore the formation of core–shell type vesicular assemblies is not expected even at low pH. These reactions also demonstrate the stability of the tetronic micelles under different experimental conditions because it is the micelle surface cavities which are involved in the synthesis of AuNPs and without the formation of such cavities reaction cannot be initiated.

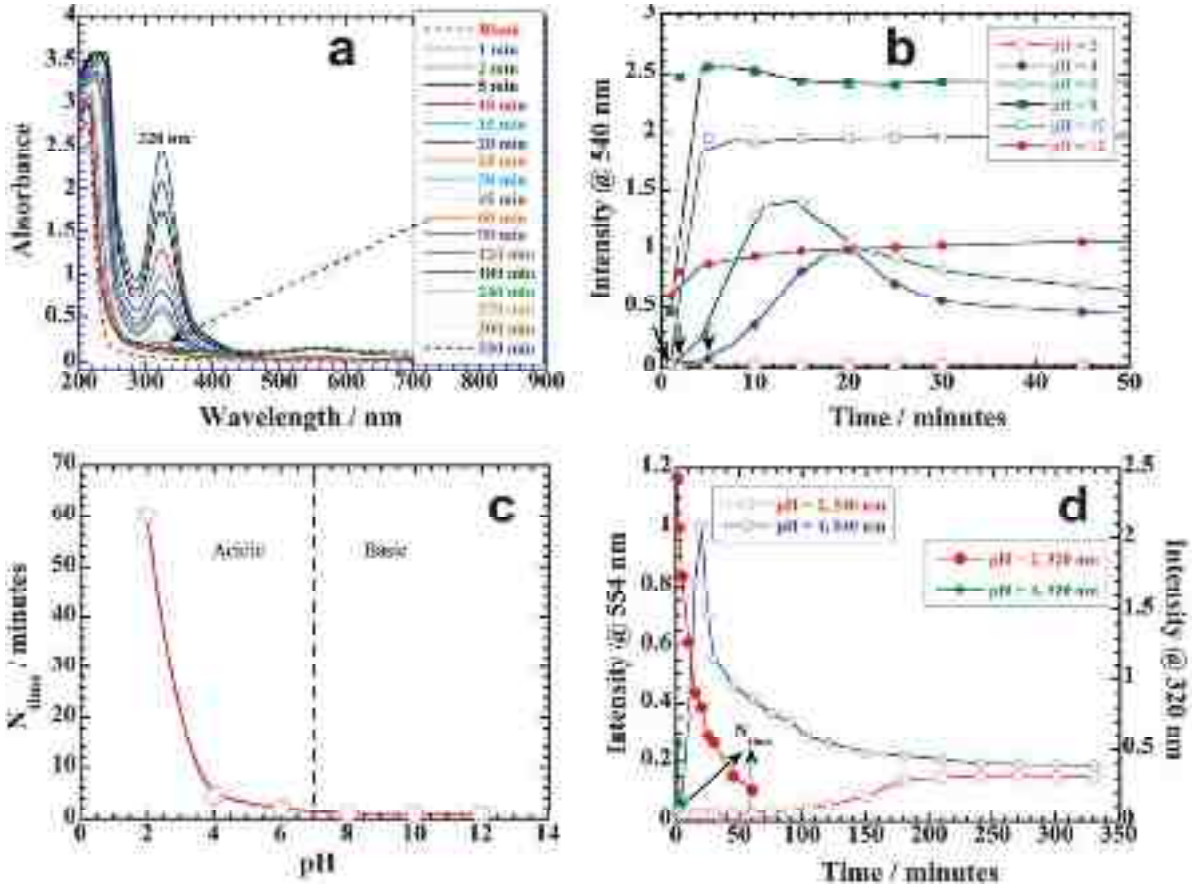

Figure 3: (a) A typical example of a reaction in the aqueous phase of 10 mM T904 with 0.5 mM HAuCl4 at pH = 2 under the effect of reaction time over 330 minutes and simultaneously monitored by the UV-Visible measurements. Red dotted line refers to blank (i.e. aqueous 10 mM T904 without gold salt) and blue dotted line represents the scan at 330 minutes of the reaction. (b) Shows the variation of intensity of 540 nm peak versus time for the same reaction at different pH values. Arrows represent the time required for the initiation of the nucleation temperature (N_{time}) from where the synthesis of gold nucleating centres starts. (c) Plot of N_{time} versus pH for the reactions at different pH for T904. (d) Comparison of the intensity variation of LMCT complex at 320 nm and gold nucleating centres at 540 nm at pH 2 and 4. It shows that when the intensity of peak 320 nm diminishes, then the intensity of corresponding gold nucleating centres at 540 nm starts. Arrows indicate the time when this happens for two reactions conducted at pH = 2 and 4.

Additive effect

In order to further authenticate that the tetronic micelles directly control the reduction of Au(III) into Au(0) and subsequent formation of AuNPs, we carried out the measurements in the presence of different additives which can stabilize or destabilize the T904 micelles and hence consequently affect the synthesis of AuNPs. For this purpose, a reaction conducted at pH = 4 (Fig. 2b) has been taken as control to demonstrate the additive effect. First, we took a series of nonionic surfactants (octaethyleneglycol monodecyl ether C10E8, tetraethyleneglycol monododecyl ether C12E4, and octaethyleneglycolmonotetradecyl ether C14E8) as additives, and Fig. 4a shows the variation in the absorbance of Au NPs at 540 nm in the presence of different amounts of C14E8. The N_T thus calculated in the presence of each surfactant is plotted in Fig. 4b. 5 mM amount of each nonionic surfactant initially reduces the N_T, but further increase in the amount increases the N_T. This explains

that 5 mM of nonionic surfactant in fact stabilizes the T904 micelles by forming stable mixed micelles and hence micelle formation occurs at a relatively low temperature which in turn reduces the N_T. This is not expected for 10 and 20 mM of the nonionic surfactant because the amount of T904 used is 10 mM. Thus, a higher temperature is required to induce micellization which consequently leads to an increase in N_T because nonionic surfactants are not expected to participate in the reduction of Au(III) into Au(0). However, the overall N_T values decrease in the order of C10E8 > C12E4 > C14E8, which is the order of their increase in hydrophobicity, because greater hydrophobicity of the additive induces greater dehydration and hence micelle formation occurs at lower temperatures. On the other hand, the additive effect of a series of anionic surfactants causes a decrease in N_T (Fig. 4b) because T904 is considered to be predominantly protonated at pH = 4 and hence will exhibit electrostatic interactions with an anionic surfactant. Charge neutralization followed by increasing hydrophobicity in the order of sodium dodecyl sulfate (SDS), sodium tetradecyl sulfate (STS), sodium hexadecyl sulfate SHS decreases N_T in the same order. For a series of cationic surfactants decyltrimethyl ammonium bromide (DeTAB), dodecyltrimethyl ammonium bromide DTAB, and hexadecyltrimethyl ammonium bromide HTAB), we have selected a control experiment at pH = 12 (filled circles, Fig. 2b), and the intensity versus temperature plots for the synthesis of AuNPs have been presented in Fig. 4c. The variation in N_T with respect to the number of carbon atoms in the cationic surfactant hydrocarbon tail is depicted in Fig. 4d, which increases with the increase in hydrophobicity indicating the fact that additive effect of cationic surfactant does not contribute towards the T904 micelle stability. This result is contrary to what we have observed for a series of anionic surfactants in Figure 4b where micelles are stabilized; thereby N_T decreases with the increase in hydrophobicity in the order of SDS, STS, SHS. Accommodation of the ammonium bulky head group of cationic surfactant is considered to cause unfavourable steric repulsions which further enhance with the increase in the magnitude of hydrophobicity. This induces the instability in the T904 micelle which consequently leads to an increase in the N_T.

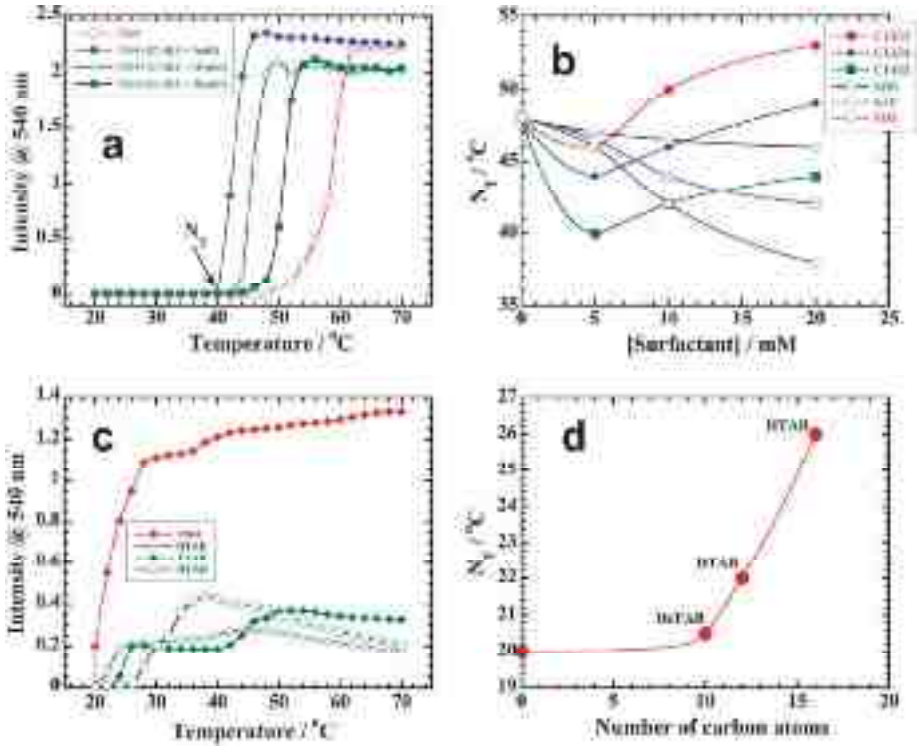

Figure 4: (a) Intensity versus temperature plots of 10 mM T904 with 0.5 mM HAuCl4 at pH = 4 under the effect of temperature variation from 20–70°C in the absence and presence of different amounts of C14E8. (b) Variation in N_T with respect to the amount of different

surfactants. (c) Shows the additive effect of hydrocarbon tail length of cationic surfactants and (d) the dependence of N_T on the number of carbon atoms in the hydrocarbon chain.

TEM studies

T904 Studies: TEM studies help us to characterize the shape and size of the AuNPs. It is also possible to evaluate the morphologies of micellar assemblies. Figure 5a–c shows the images of both AuNPs as well as micellar assemblies of the sample synthesized at pH = 4. Small black dots of Fig. 5a, close up in Figure 5b, and high resolution in Figure 5c belong to AuNPs of 17 nm, whereas large aggregated assemblies of different dimensions in light background in Fig. 5a are the vesicular assemblies of T904. If the same reaction is conducted with 1 mM of gold salt instead of 0.5 mM under identical conditions, we simply get more number of AuNPs with essentially the same size and the images are shown in Figure 5d–f. These images indicate that AuNPs are mainly adsorbed on the surface of highly hydrated compound vesicular assemblies (Figure 5d).

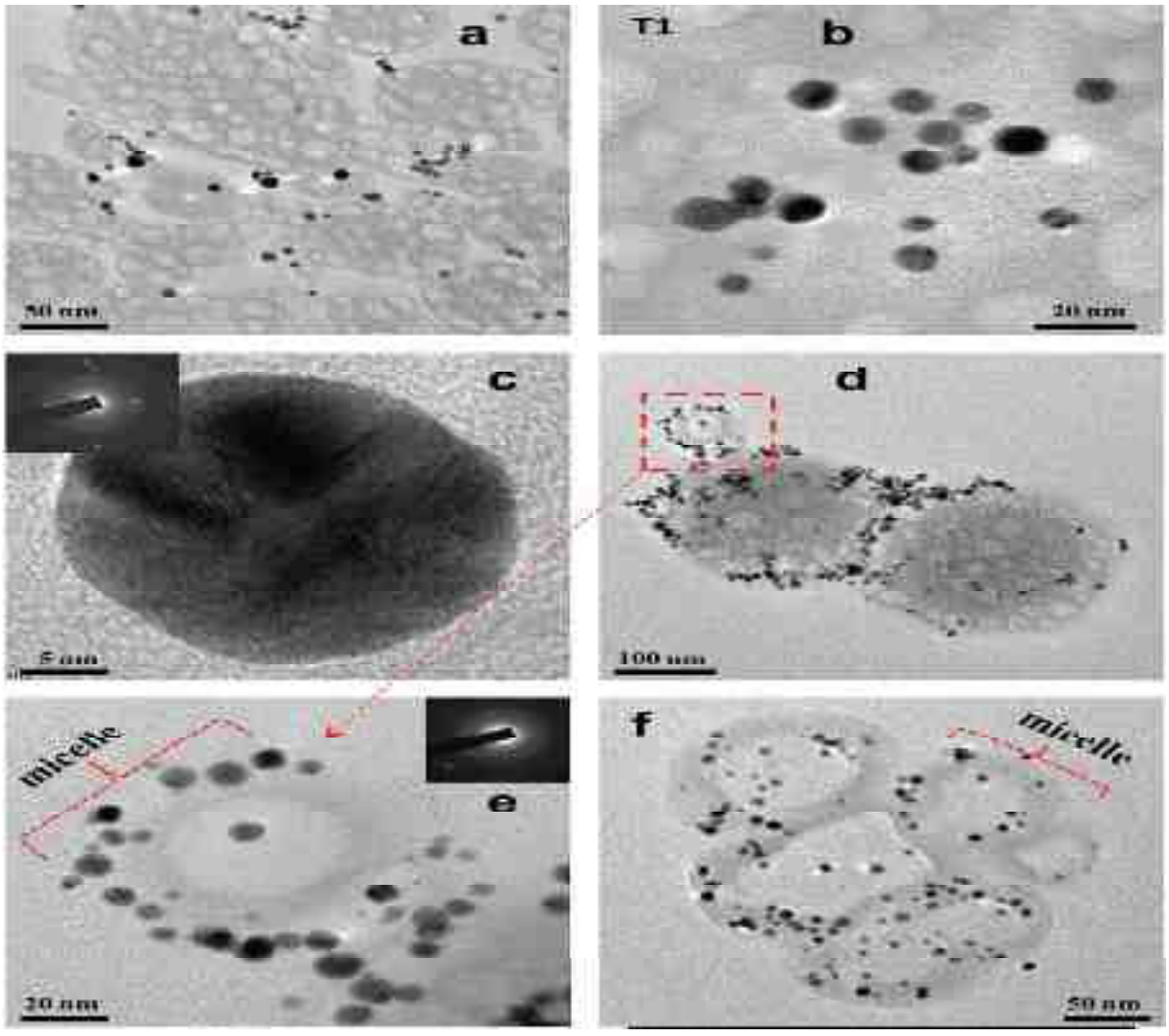

Figure 5 (a) TEM image showing large patches of vesicular assemblies of T904 along with AuNPs as dark dots of sample of Fig. 2a. Small black dots of (a), close up in (b), and high resolution in (c) are fine spherical shaped Au NPs of 17 nm. (d) Shows two sidewise fused vesicular assemblies bearing groups of small Au NPs while (e) is the high resolution image showing the presence of AuNPs mainly on the surface of the core–shell type vesicle. (f) Shows

several core–shell type vesicles fused together in a group bearing AuNPs mainly in the shell region of each vesicle.

Figure 6a–d show the images of the sample prepared at pH = 10. All images show mainly compact aggregates with no clear distinction between the core and the shell regions, hence we call them compound micelles where AuNPs of 10 nm are primarily adsorbed on their surface. A close-up image (Fig. 6d) of a single aggregate further clearly shows the presence of AuNPs on its surface without any sign of a typical core–shell type structure as observed previously for the sample prepared at pH = 4. AuNPs exist mainly in polyhedral shapes due to inter- particle fusion which is also evident from their small chain-like arrangements and is in contrast to spherical NPs of Figure 5b. Likewise, Fig. 6e–h show the images of the sample prepared at pH = 12. Again, no core–shell type morphologies are visible; rather a much compact spherical shaped compound micelles are present. Fig. 6g shows a somewhat dehydrated aggregate due to a highly basic environment at pH = 12 which prevents the protonation of amine groups and hence reduces the hydration that in turn dehydrates the micelles even at lower temperature (Figure 2c). Thus, a comparison between the samples prepared at pH = 4 (Fig. 5) and at pH = 10/12 (Fig. 6) indicates the effect of pH on the overall morphology of aggregated assemblies. pH = 4 is expected to induce excessive hydration to the protonated diamine core which facilitates the aggregation of T904 molecules in a typical core–shell vesicular structure, whereas pH = 10/12 does not allow it to happen up to this extent and hence core–shell arrangement is not visible in the images of Figure 6.

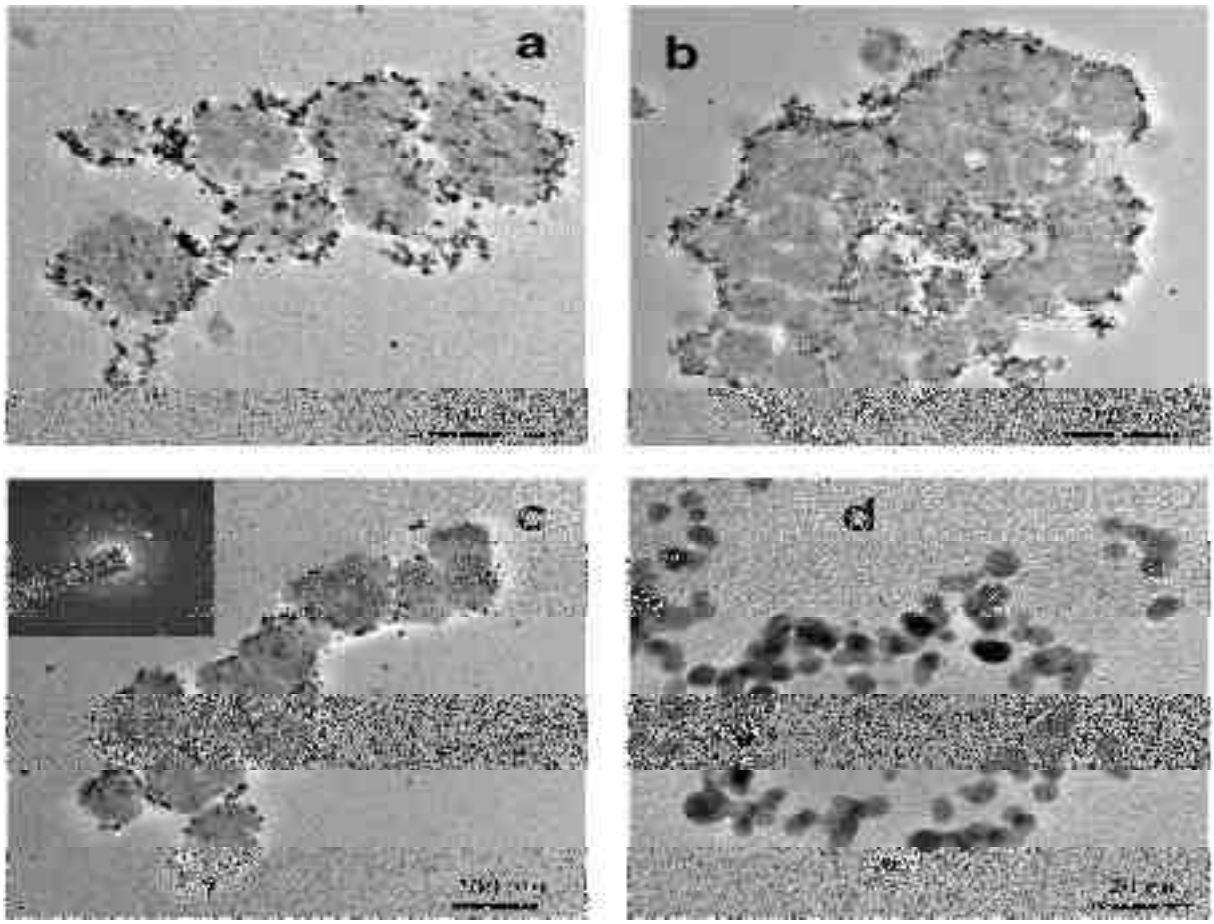

Figure 6 (a–d) TEM images of a sample prepared at pH = 10. No core–shell type vesicles are evident in contrast to the micelles of Fig. 5. All images show mainly compact micelles with

surface adsorbed Au NPs of 10 nm. (d) A close-up image of a single compact aggregate without the core and shell regions.

T908/T1307 systems

Similar morphologies are observed for T908 systems. Fig. 7 shows few images of micelles (Fig. 7a–c) and AuNPs (Fig. 7d) for a sample prepared at pH = 4. The micelles are slightly larger (~200 nm) than those of T904 due to a much larger PEO block (EO = 114) of T908 in comparison to that of T904 (EO = 15) but no core–shell type vesicular morphologies are observed. Apart from this, AuNPs of specific shapes (see triangles and hexagons in Fig. 7d) are present rather than of roughly spherical shapes of Fig. 5b. For T1307 systems, one can see spindle shaped compound micelles (Fig. 8a) apart from roughly

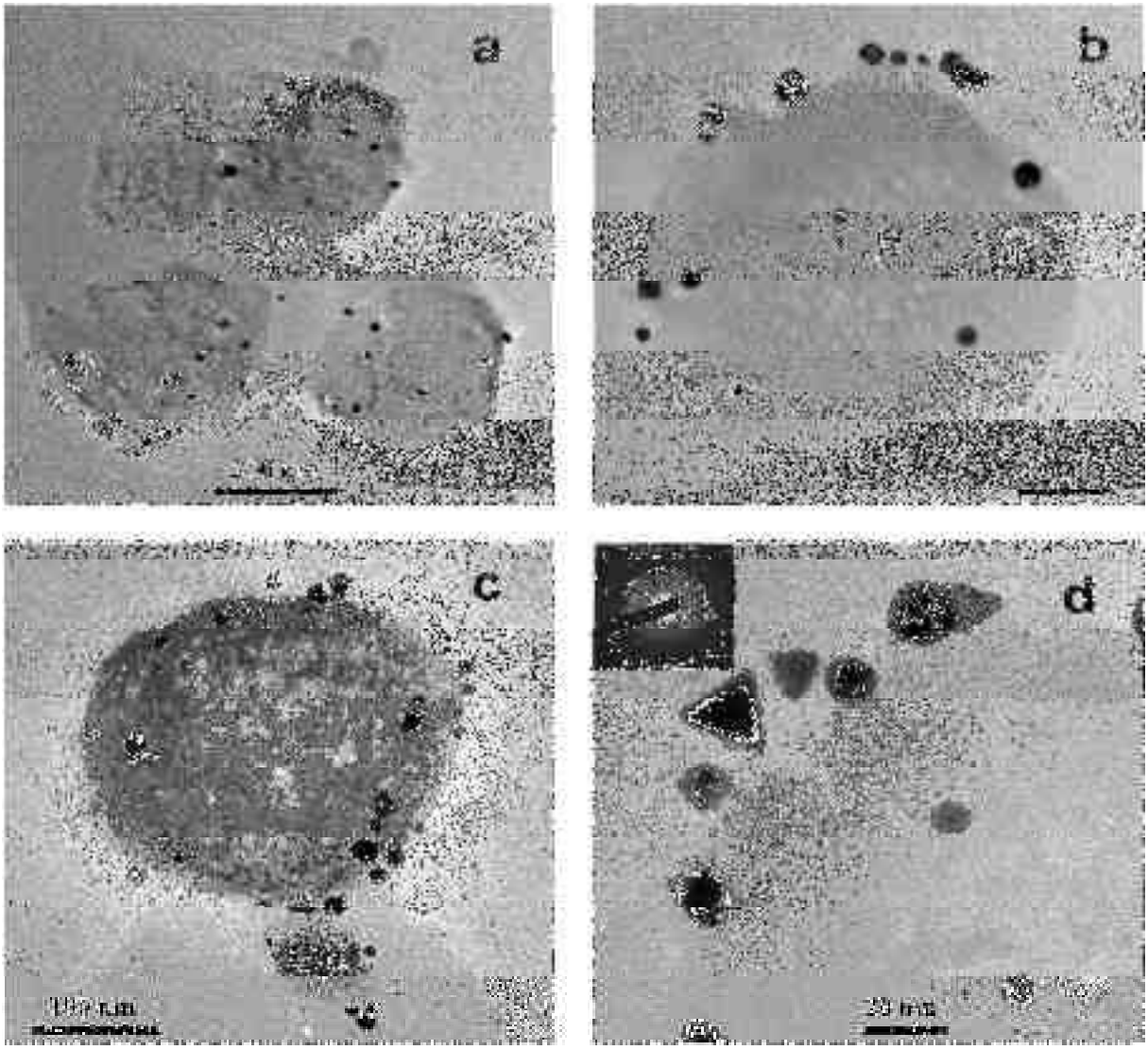

Figure 7 (a–d): TEM images of large compound micelles of T908 bearing AuNPs prepared at pH = 4. (a) Shows a group of compound micelles whereas (b) and (c) show different compound micelles with surface adsorbed AuNPs. (d) A high resolution TEM image of a part of micelle bearing small NPs of different shapes

spherical ones (Fig. 8b and c) along with a few fused (Fig. 8d and e) micelles. PPO block with PO = 32 of T1307 is the largest among present tetronics and could be responsible for other non-spherical shapes and also induces polydisperse behavior that produces compound micelles of different sizes. For instant, the micelles of less than 50 nm bear few AuNPs (see dotted circles in Fig. 8b and c) due to their smaller size, in contrast to large compound micelles (Fig. 8e and f) which bear several small AuNPs on their surface. The absence of core–shell type morphologies in the samples of T908 and T3107 can be explained on the basis of the hydrophilic–lipophilic balance (HLB) and the ratio between the Flory radius of the PPO and PEO blocks (β). $\beta = [I_{PO} (N_{PO})^{3/5} / I_{EO}(N_{EO})^{3/5}]$, where N_{PO} and N_{EO} are the numbers of PO and EO units, respectively, and I_{PO} and I_{EO} are the corresponding lengths of the PO (5.1 Å) and EO (2.4 Å) units**.** HLB and β values for T904, T908, and T1307 are 12–18, >24, >24 and 2.29, 0.77, 1.07, respectively. A β value close to 1 and HLB greater than 18 refer to highly hydrophilic tetronics of T908 and T1307, while β greater than 1 and HLB less than 18 suggest the presence of a predominantly hydrophobic nature with inter- mediate polarity of T904. This is obviously understood from the greater number of PO units than EO in T904 (EO = 15, PO = 17) while reverse is true for T908 (EO = 114, PO = 21) and T1307 (EO = 72, PO = 32). Thus, the lesser number of EO units in comparison to PO in T904 makes it predominantly hydrophobic which compels T904 to adopt a core–shell type aggregated morphology at low pH when protonated diamine groups are highly hydrated. In contrast, at high pH, excessive hydration of amine groups is prevented and hence T904 acquires regular micellar shape in which predominantly PPO blocks occupy core of the micelle and that is why we see only compound micelles without any core–shell type morphologies. T908 and T3107 are highly hydrophilic polymers because of much greater number of EO units than PO, therefore the formation of core–shell type vesicular assemblies is not expected even at low pH.

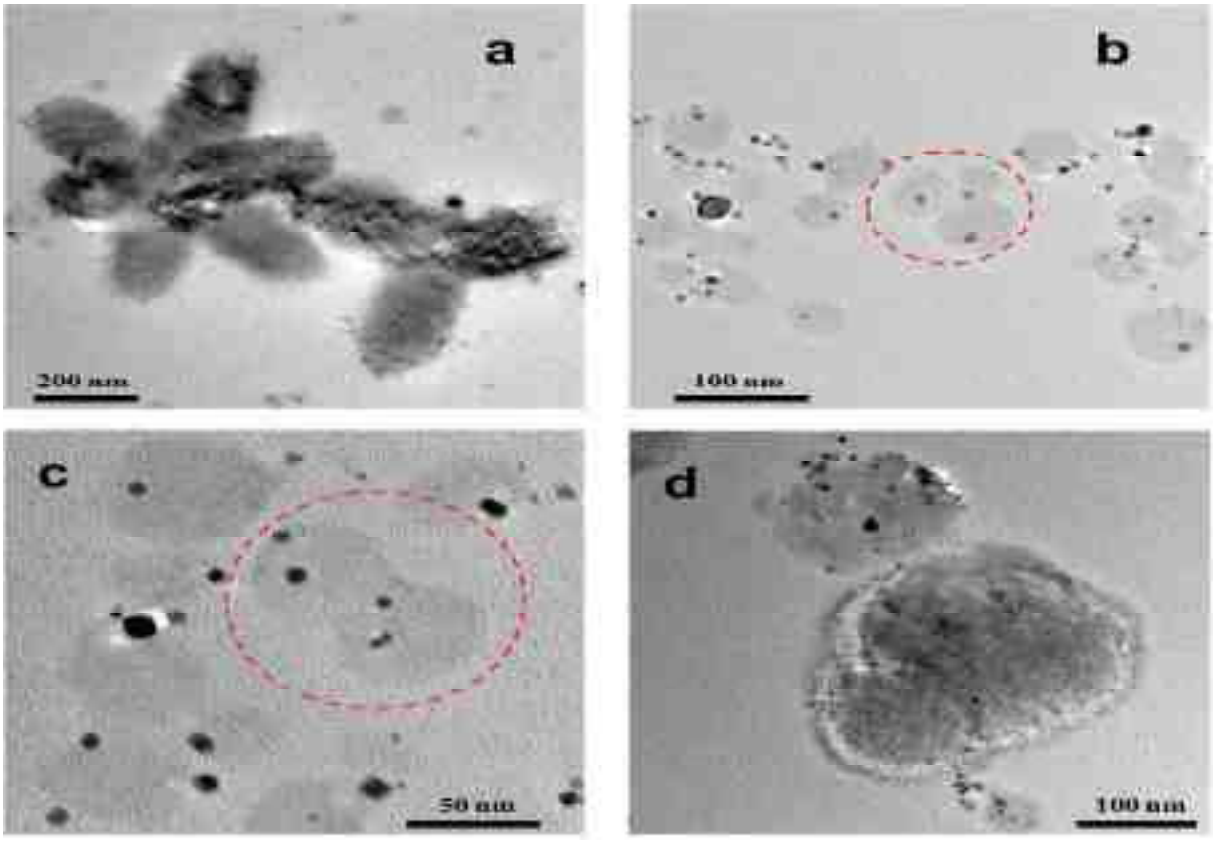

Fig. 8 (a) TEM image of spindle shaped compound micelles. (b) and (c) Show roughly spherical micelles with Au NPs.

From the above results, we conclude that the micelles of tetronics are highly responsive to the pH and temperature variations. The origin of pH responsive behavior is attributed to the diamine functional groups of tetronic macromolecules which in turn produced pH sensitive micelles. The presence of ether oxygens in the PEO and PPO blocks along with quaternary amine functional groups at low pH drive water molecules to induce micelle hydration; hence, these micelles are much more temperature sensitive than the micelles produced at high pH.

2. pH Effect on the Adsorption of Amino Acids on Gold Nanoparticles

Colloidal solution of AuNPs of concentration 0.5 mM is prepared. In a typical synthesis, 25 ml of the 0.5 mM $HAuCl_4$ is mixed with 5 mM tri-sodium citrate in triply distilled water. This solution is then vigorously stirred for 30 minutes. To this solution, 0.6 ml of freshly prepared $NaBH_4$ having concentration 0.002 M is added drop wise with constant stirring for about 1 minute. This prepared solution is then kept undisturbed overnight. This prepared solution is characterized using UV-Vis spectrometer showing SPB at approximately 520 nm. All the three amino acids (AAs) (L-Arginine (Arg), L-Glutamic acid (Glu) and L-Cysteine (Cys)) of concentration 1 mM are prepared separately in triply distilled water. 1 mM of each AA is taken in four separate 20 ml vials. The pH of each vial is adjusted as 5, 7, 9 and 11, respectively. Similarly, Au sol is also taken in four vials and pH of each is adjusted as 5, 7, 9 and 1, respectively. The Au colloidal solution and the AA with adjusted pH separately are then mixed in 9:1(v/v) ratio, respectively. The time effect is measured with UV-visible spectrometer at a resolution of 1 nm and within the 200 nm to 800 nm wavelength range.

RESULTS AND DISCUSSION

Structure and Morphology: The Au sol is stabilized by anionic citrate molecules, which are adsorbed on the positively charged AuNPs surface at different pH values, where citrate molecules itself undergo protonation. On addition of Cys at pH 5 to 11, the thiol group undergoes strong and thermodynamically favourable covalent bond formation with Au surface. To understand the role of Cys in the colloidal Cit-AuNPs sol, a complete picture can be evaluated from wavelength versus time (Fig. 1) and intensity @ 540 nm versus time (Fig. 2) plots at different pH of Cys-AuNPs.

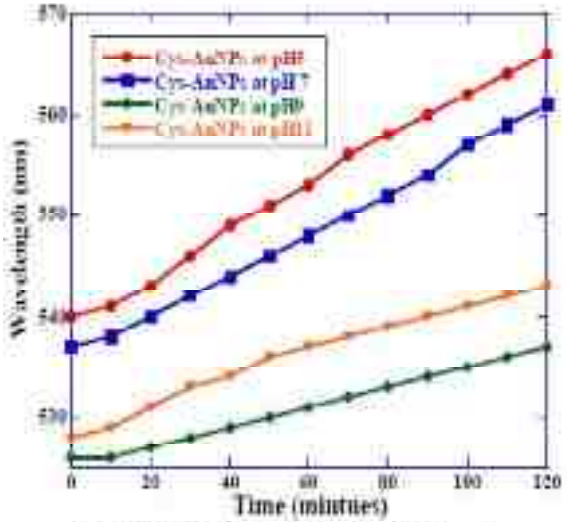

Fig. 1: Wavelength versus reaction time plot of Cys-Au NPs at different value of pH.

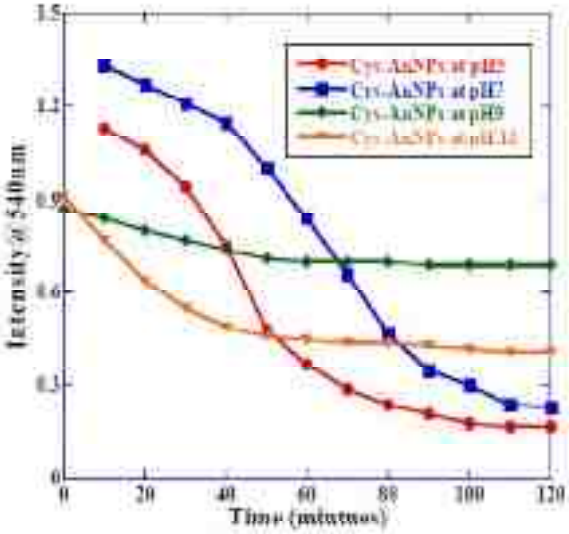

FIG. 2: Intensity @ 540nm versus reaction time plot of Cys-Au NPs at different value of pH.

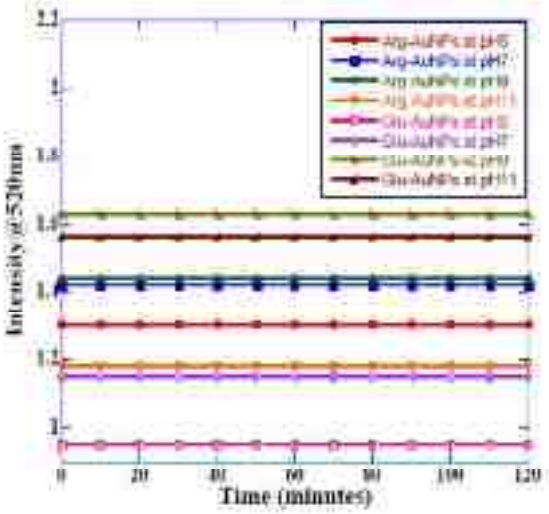

FIG. 3: Intensity@520nm versus reaction time plot of Arg-Au NPs and Glu-Au NPs at different value of pH.

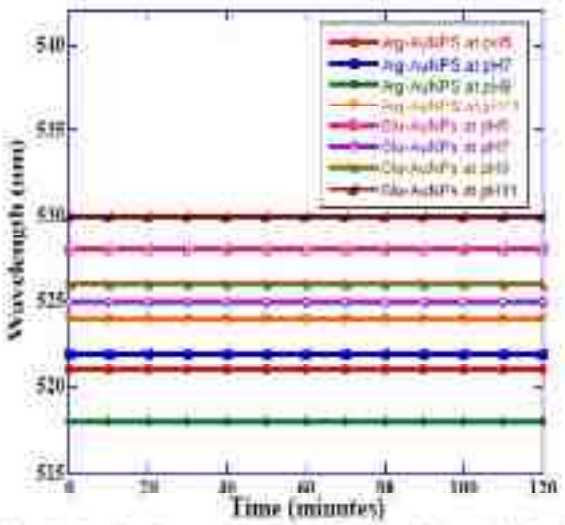

FIG. 4: Wavelength versus reaction time plot of Arg-Au NPs and Glu-Au NPs at different value of pH.

At pH 5, 7 (Fig. 1), SPR peak increases from 540 nm to 566 nm and from 537 nm to 561 nm, respectively. Further at pH 9, 11(Fig. 1), SPR peak increase from 526 nm to 538 nm and 528 nm to 544 nm, respectively. The more increase of λ_{max} with time are associated with aggregation at pH 5 and pH 7. Moreover, at pH 5 and pH 7, plasmon coupling occurs due to the formation of inter NP bridges due to H-bonding between NH_3^+ present on one Cys-AuNPs surface and COO^- of other Cys-AuNPs surface. Further on additions of Cys at pH 9 and pH 11, -SH group will replace citrate group, thus absorbed on the surface of Au NPs and NH_2 (due to pH 9, 11) and COO^- groups will remain the surface. Fig. 2 shows the change in intensity@540nm versus time plot. Both the plots wavelength and intensity versus time support each other. As wavelength increases, intensity of the corresponding pH of Cys-Au NPs samples decreases, which is associated with the displacement of citrate molecules with –SH group of Cys at various pH values. In Arg-Au NPs and Glu-Au NPs, SPB remains same ~ 520 nm at all pH values (Fig. 3). Moreover, at a particular pH, there is no change in wavelength with time (Fig. 4), which indicates that Arg-Au NPs and Glu-AuNPs are more stable. In the case of Glu-AuNPs, no aggregation is seen at various pH values from 5 to 11. This may be attributed to two COO^- groups of Glu, which stabilize the Au NPs with similar interactions as COO^- groups of Cit molecule adsorbed on AuNPs surface. Similarly, in the case of Arg-AuNPs, one of the amine acts as primary amine can interact with AuNPs again through weak covalent bonds along with COO^- of Arg and Cit molecules.

3. Understanding the Mechanism of Adsorption of Cethyltrimethyl ammonium Bromde (CTAB) and Polylysine (PLL) on Silver Nanoparticles and Detection of Hg^{2+}

$AgNO_3$ (1 mM) is dissolved in distilled water. On addition of PLL (Figure 1) (0.35 ml) into it, color of the solution is changed from colorless to yellow. Stir the solution for 10 minutes at 70°C. Then, CTAB (Figure 1) (0.25 mM) is added into the above stirred solution. Final pH of solution is 6.3. The initial color of the solution is changed from yellow to brown within 3 hours without any suspension. After 3 hours, the sample is cooled to room temperature and kept overnight. Purification of the sample is done with pure water at least two times to remove unreacted PLL and CTAB. AgNPs are centrifuged at 14,000 rpm for 5 minute. AgNPs are collected after washing

each time with distilled water. Series of reactions have been carried out by varying the concentration of reactant precursor such as [$AgNO_3$] = 0.5 mM, 1 mM, 2 mM; [PLL] = 0.26 ml, 0.35 ml, 0.44 ml and [CTAB] = 0.2 mM, 0.25 mM, 0.3 mM.

AgNPs are formed on the addition of PLL to $AgNO_3$. It is confirmed from the change in color of the solution from colorless to turbid brown with suspension, which is also supported from broad SPR band in UV-Visible spectra. SPR band originates due to collective oscillations of electrons owing to their interaction with incident electromagnetic radiations, thus, SPR band of nano sized Ag particles indicate absorbance in UV-Visible region at 420 nm. The quality of NPs can be estimated from the pattern of absorbance peak. Sharp peak indicate small size NPs having narrow size distribution though the broader peak represent the NPs with wide size distribution. Thus, in the present study, the stability of AgNPs is determined by using CTAB. Reduction of $AgNO_3$ using PLL in the presence of CTAB is carried out at a temperature ranging from 20°C to 70°C (Figure 2a). Aqueous PLL in the presence of CTAB remains in the native state upto 40°C. Further increase in temperature from 50°C to 60°C results in the appearance of a peak at λ_{max}= 450 nm, indicating the presence of AgNPs. Here, 70°C is considered to be the suitable temperature, where PLL shows its maximum reduction potential in the presence of CTAB. The absorbance around λ_{max} = 450 nm becomes prominent only around this temperature. Therefore, in order to understand the whole mechanism, set of reactions have been carried out by varying the concentration of PLL, CTAB and $AgNO_3$ at 70°C.

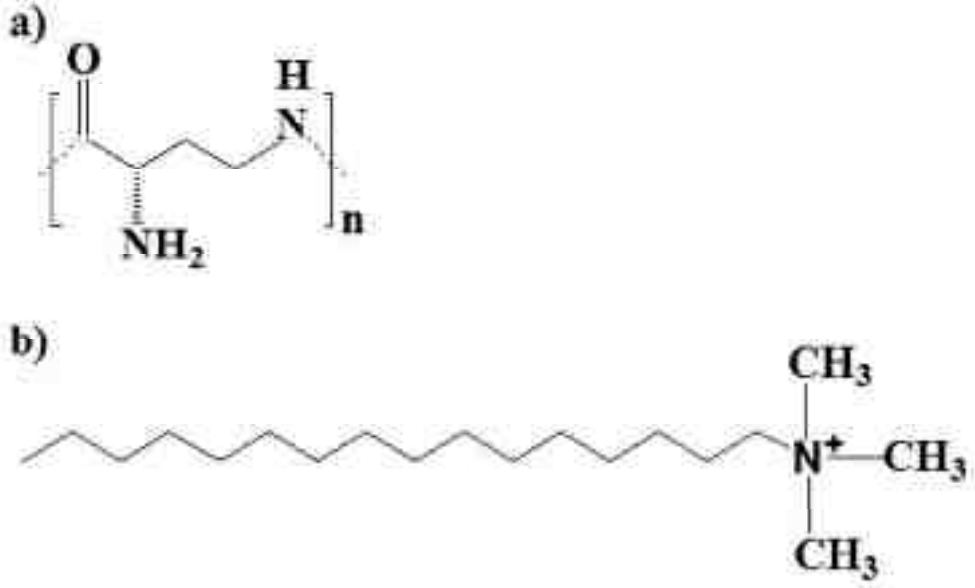

Figure1: Structure of a) PLL and b) CTAB.

Effect of concentration of CTAB on AgNPs Synthesis

The concentration of [CTAB] = 0.2 mM, 0.25 mM and 0.3 mM is varied by keeping [$AgNO_3$] = 1 mM and [PLL] = 0.35 ml to be constant. At [CTAB] = 0.20 mM, solution is brown indicating the formation of AgNPs. However, suspension appears after 5 hours. At [CTAB] = 0.25 mM (Figure 2b), the color of the solution remains brown, which is stable with no suspension. At [CTAB] = 0.30 mM, brown color with suspension appears in 3 hours of reaction. In UV-Visible plots of absorbance vs. wavelength, the absorbance increases while wavelength decreases as λ_{max} = 461 nm, 450 nm and 435 nm with increase in the concentration of [CTAB] = 0.2 mM, 0.25 mM and 0.3 mM, respectively.

Plot of intensity at λ_{max} = 460 nm versus time (Figure 2c) indicates the effect of different concentration of CTAB on the fabrication of AgNPs using PLL at constant temperature. The greater magnitude of the curve is in line with the greater number density of NPs produced. PLL-AgNPs has much lower magnitude of SPR band in comparison to that in the presence of CTAB. It signifies that

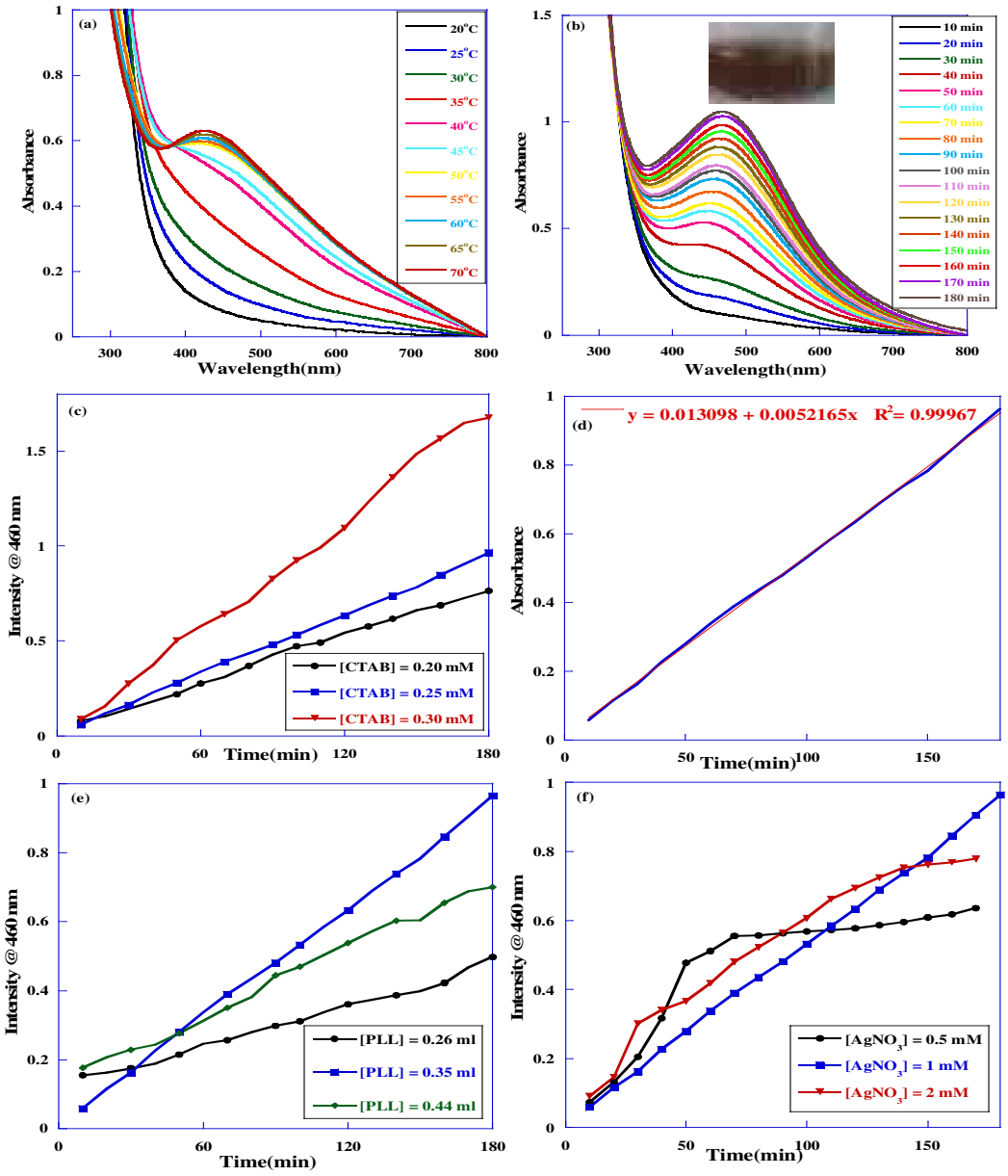

Figure 2 (a)Absorbance versus wavelength scan of [$AgNO_3$] = 1 mM; [PLL] = 0.35 ml; [CTAB] = 0.25 mM with respect to reaction temperature from 20°C to 70 °C (b) UV-Visible spectra of $AgNO_3$+PLL+CTAB mixture at 70°C with [$AgNO_3$] = 1 mM ; [PLL] = 0.35 ml and [CTAB] = 0.25 mM (c) intensity @ 460 nm versus reaction time, respectively for different mixtures keeping [$AgNO_3$] = 1 mM; [PLL] = 0.35 ml to be constant and [CTAB] = 0.20 mM, 0.25 mM, 0.30 mM. Similarly plots of (d) Absorbance versus time plot for [$AgNO_3$] = 1 mM; [PLL] = 0.35 ml; [CTAB] = 0.25 mM by selecting maximum points to find linear regression coefficient (e) Intensity @ 460 nm versus reaction time, respectively for different mixtures keeping [$AgNO_3$] = 1 mM; [CTAB] = 0.25 mM to be constant and [PLL] = 0.26 ml, 0.35 ml, 0.44 ml (f) Intensity @ 460 nm versus reaction time, respectively for different mixtures keeping [CTAB] = 0.25 mM; [PLL] = 0.35 ml to be constant and [$AgNO_3$] = 0.5 mM, 1 mM, 2 mM.

the reduction is expedited in the presence of CTAB and least in its absence, i.e. in aqueous PLL only. Moreover, magnitude of the curve increases with an increase in the concentration of CTAB from 0.2 mM to 0.3 mM. We consider [CTAB] = 0.25 mM to be the best concentration, where AgNPs are the most stable without aggregation. However, at [CTAB] = 0.3 mM plot, there is increase in intensity with time, which is attributed not only to greater number density of AgNPs but a secondary process of complexation of PLL and CTAB might takes place. As a result, a blank experiment to determine that complexation between PLL and CTAB has been carried out. PLL and CTAB show an edge around 215 nm each, whose intensity increases on mixing both of them. An increased intensity is related to the formation of complex between PLL and CTAB. Thus, at [CTAB] = 0.25 mM, the amount of CTAB is sufficient to stabilize AgNPs, however at [CTAB] = 0.3 mM, CTAB not only stabilize AgNPs but also form a complex with PLL, as a result SPR band becomes flat with increased intensity. It could be further explained in a way as PLL shows different conformation in aqueous solution above 40°C. The dominant conformation of PLL is random coil due to repulsion among protonated lysine residues. However, in our case, 0.1% PLL in water, PLL undergoes acid-base equilibrium as

$$NH_3^+ + H_2O \longrightarrow NH_2$$

Deprotonated NH_2 allows the existence of alpha helix structure. However, β-sheet structure appears above 40°C, in which NH_2 sites are available to interact with Ag(I). As a result PLL act as a reducing agent, hence SPR band starts appearing indicating the formation of Ag(0). Now, as the concentration of CTAB increases, it interacts with the adsorbed PLL tails, leading to the conformational changes in the adsorbed polymer. Moreover, more and more CTAB molecules and micelles go into folded chains that stretch more loops further. The stretching is expected to continue until the coils are saturated with adsorbed CTAB micelles and molecules. The conformational changes are based on the ion pair formation between electron pair of NH_2 and positively charged head group of CTAB molecules, which brings a positively charged trimethylammonium group in the vicinity of AgNPs. The mechanism is also illustrated in Scheme 1.

First order rate constant values are 4.14 x 10^{-3} s^{-1}, 5.21 x 10^{-3} s^{-1}, 9.79 x 10^{-3} s^{-1} for [CTAB] = 0.2 mM, 0.25 mM, 0.3 mM. These are calculated by choosing maximum points from the data. The plot with maximum points for [CTAB] = 0.25 mM with linear regression coefficient R^2 = 0.99967 is shown in Figure 2d.

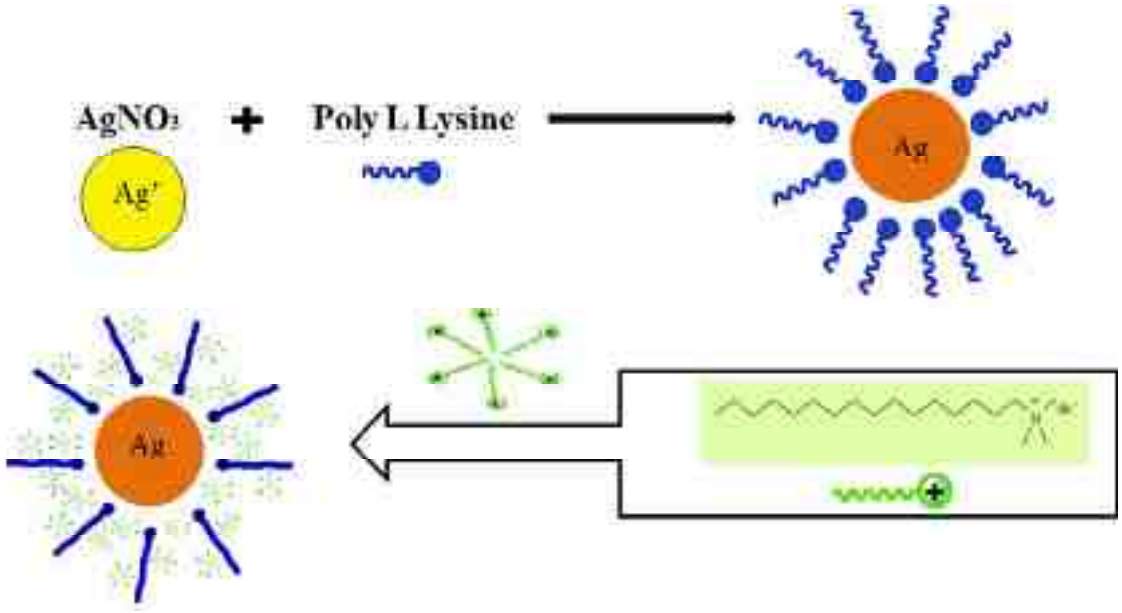

Scheme 1:A schematic illustration of the fabrication process of PL-CT-AgNPs.

Effect of Concentration of PLL on AgNPs synthesis

To determine the effect of PLL on AgNPs synthesis, UV-Visible plots of wavelength vs absorbance are taken at different amounts of PLL = 0.26 ml, 0.35 ml, 0.44 ml keeping [$AgNO_3$] = 1mM and [CTAB] = 0.25 mM to be constant. The solution becomes muddy brown with suspension within 3 hours at [PLL] = 0.26 ml and 0.44 ml. At [PLL] = 0.35 ml (Figure 2b), solution turns to brown having λ_{max}= 450 nm with no suspension. Thus, adsorption of PLL along with CTAB at a particular concentration leads to the stabilization of AgNPs.

Intensity @ 460 nm vs time is plotted as shown in Figure 2e. Intensity increases from PLL = 0.26 ml to 0.35 ml, which directly indicates the greater number of AgNPs formed. Moreover, at PLL = 0.44 ml, magnitude of the intensity again decreases and peak become flattened. Thus, an increase in intensity at PLL = 0.35 ml is related to the facilitation of reduction of Ag(I) to Ag(0). In each case, synthesis of AgNPs begins within 5 minutes of the reaction time, thus depicting the maximum reduction potential of PLL. First order rate constant values are 1.9 x $10^{-3}s^{-1}$, 5.21 x $10^{-3}s^{-1}$, 3.31 x $10^{-3}s^{-1}$for [PLL] = 0.26 ml, 0.35 ml, 0.44 ml, respectively. The plot with maximum points for [PLL] = 0.35 ml with linear regression coefficient R^2 = 0.99967 is shown in Figure 2d. These values support that PLL= 0.35 ml is the most suitable amount for the reduction of Ag(I) to Ag(0) along with CTAB.

Effect of concentration of $AgNO_3$ on AgNPs synthesis

For this, we have taken different concentration of [$AgNO_3$] = 0.5 mM, 1 mM, 2 mM keeping [PLL] = 0.35 ml and [CTAB] = 0.25 mM to be constant. UV-Visible plots at all concentrations have been taken. At [$AgNO_3$] = 0.5 mM solution has light brown color with suspension and at higher concentration i.e. [$AgNO_3$] = 2 mM solution has brown color with suspension within 3 hours of reaction. [$AgNO_3$] = 1mM (Figure 2b) is the most suitable concentration with brown color and no suspension.

Intensity @ 460 nm vs time is plotted as shown in Figure 2f. Intensity increases from [$AgNO_3$] = 0.5 mM to 1 mM, which directly indicates the greater number of AgNPs formed. Moreover, at [$AgNO_3$] = 2 mM, magnitude of the intensity again decreases. Thus, an increase in intensity at [$AgNO_3$] = 1 mM indicates that it is the most appropriate concentration for the reduction of Ag(I) to Ag(0) in the presence of PLL and CTAB. First order rate constant values are calculated and are 0.9 x $10^{-3}s^{-1}$, 5.21 x $10^{-3}s^{-1}$, 4.32 x $10^{-3}s^{-1}$for [$AgNO_3$] = 0.5 mM, 1 mM, 2 mM, respectively. The plot with maximum points for [$AgNO_3$] = 1 mM with linear regression coefficient R^2 = 0.99967 is shown in Figure 2d. The rate constant values for different concentrations of CTAB, PLL and $AgNO_3$ calculated from the plots further support the results. The contour of the curve in each case (Figure 2c, Figure 2e and Figure 2f) exhibits the nature of reaction kinetics. The plots of absorbance versus time clearly indicate that the formation of silver sol has an induction period (nucleation) followed by autocatalysis (growth). Nucleating centers thus created undergo an instant growth process, which is indicated by sharp rise in absorbance in all plots.

TEM and XRD

The morphology and size of AgNPs prepared using PLL and CTAB is determined from TEM analysis. The TEM images revealed the formation of spherical particles with a thin and tight layer of PLL coated over it, denoted by an arrow in Figure 3a. The size distribution histogram reveals the average particle size to be 20 nm for polylysine and CTAB coated AgNPs (PL-CT-AgNPs) (Figure 3b).

The XRD patterns of as formulated PL-CT-AgNPs are shown in Figure 3c, revealing the crystalline phases of NPs. The peaks at 2Θ = 38.3, 44.6, 64.7 and 77.5 are indexed as planes for AgNPs. The results are to be consistent well with the reported standards (JCPDS file no. 04-0784).

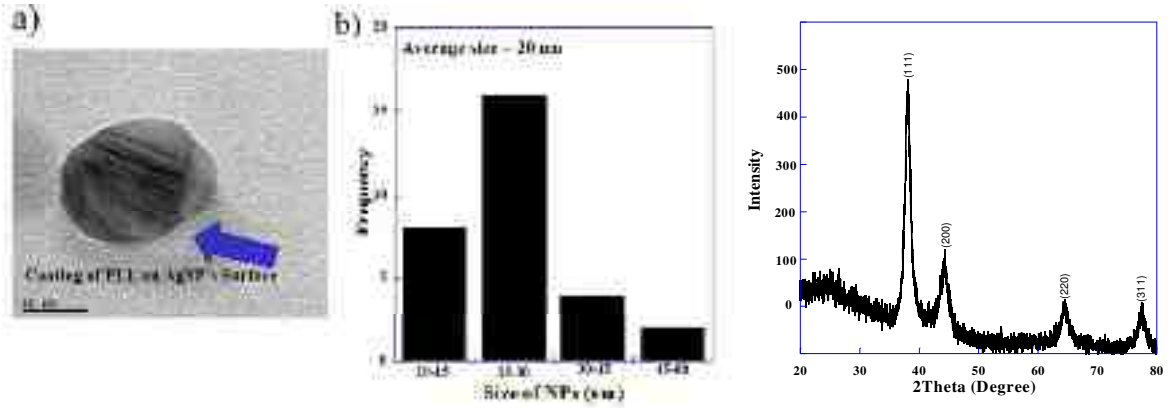

Figure 3: TEM image of PL-CT-AgNPs. Blue arrow shows a thin layer coating of PLL around each NP. The scale bar corresponds to 10 nm (b) Bar graph showing corresponding particle size distribution of PL-CT-AgNPs (c) XRD spectrum illustrating the crystalline nature of PL-CT-AgNPs.

Metal Ion Recognition ability of PLL-AgNPs

PL-CT-AgNPs in the present study is probed for their usage as a colorimetric sensor for the detection of metal ions. The metal ions detection ability of PL-CT-AgNPs is studied for each of the metal ions separately comprising Al(III), Cr(III), Hg(II), Sr(II), Ca(II), Zn(II), Ni(II), Cu(II),Cd(II), Co(II), Mg(II), Mn(II) and Ag(I) at a fixed concentrations of 200 μM. The variation in intensity of absorbance is examined using UV-Visible spectroscopy. The intensity of the SPR band and color of the solution does not show any significant change upon addition of various metal salts to PL-CT-AgNPs solution. However, upon addition of Hg^{2+}, the color of the solution changed from brown to colorless. Thus, a significant decrease in the intensity of SPR band is observed demonstrating the high sensitivity of PL-CT-AgNPs towards Hg^{2+}. The change in absorption intensity after the addition of different metal ions to the PL-CT-AgNPs solutionis demonstrated in Figure 4a.

To further investigate the ability of Hg^{2+} ions to bind with PL-CT-AgNPs, titration is performed by adding small aliquots of Hg^{2+} to AgNPs under the similar laboratory conditions. The successive addition of Hg^{2+} (from 0 μM to 200 μM) to PL-CT-AgNPs in which the SPR band of the system is examined with UV-Visible spectroscopy. There is gradual hypochromic effect in its SPR band upon addition of Hg^{2+} ions to PL-CT-AgNPs solution. The decrease in intensity depends upon the concentration of Hg^{2+} ions in the solution. This could be attributed to a direct redox reaction between zero valent Ag and Hg^{2+} ions, where AgNPs are oxidized to form Ag^{+} and Hg^{2+} ions are reduced to Hg, moving away the coating of PLL and CTAB from the surface of AgNPs. It is attributed to the differences in the standard potential of 0.8V (Ag^{+}/Ag) and 0.85V (Hg^{2+}/Hg). The absorption intensity decreased with increased concentration of Hg^{2+} ions ranging from 0 to 200 μM. The value of linear regression coefficient (R^2) is found to be 0.9999 with the detection limit upto 43 μM. To investigate the selectivity of PL-CT-AgNPs for Hg^{2+} ions, competitive metal binding experiments are also performed, to estimate Hg^{2+} in the presence of Cr^{3+}, Cd^{3+}, Cu^{3+}, Co^{3+}, Zn^{2+}, Sr^{2+}, Mg^{2+}, Al^{3+} ,Mn^{2+}, Ca^{2+} Ag^{1+} and Ni^{2+}. For this, aqueous solution of Hg^{2+} and other metal ions having concentration 100 μM each is spiked into aqueous solution of PL-CT-AgNPs. There is no change in the absorbance of Hg^{2+} - PL-CT-AgNPs solution on addition of other metal ions (Figure 4b). Thus, the results indicate that PL-CT-AgNPs possesses good selectivity toward Hg^{2+} in the presence of other metal ions.

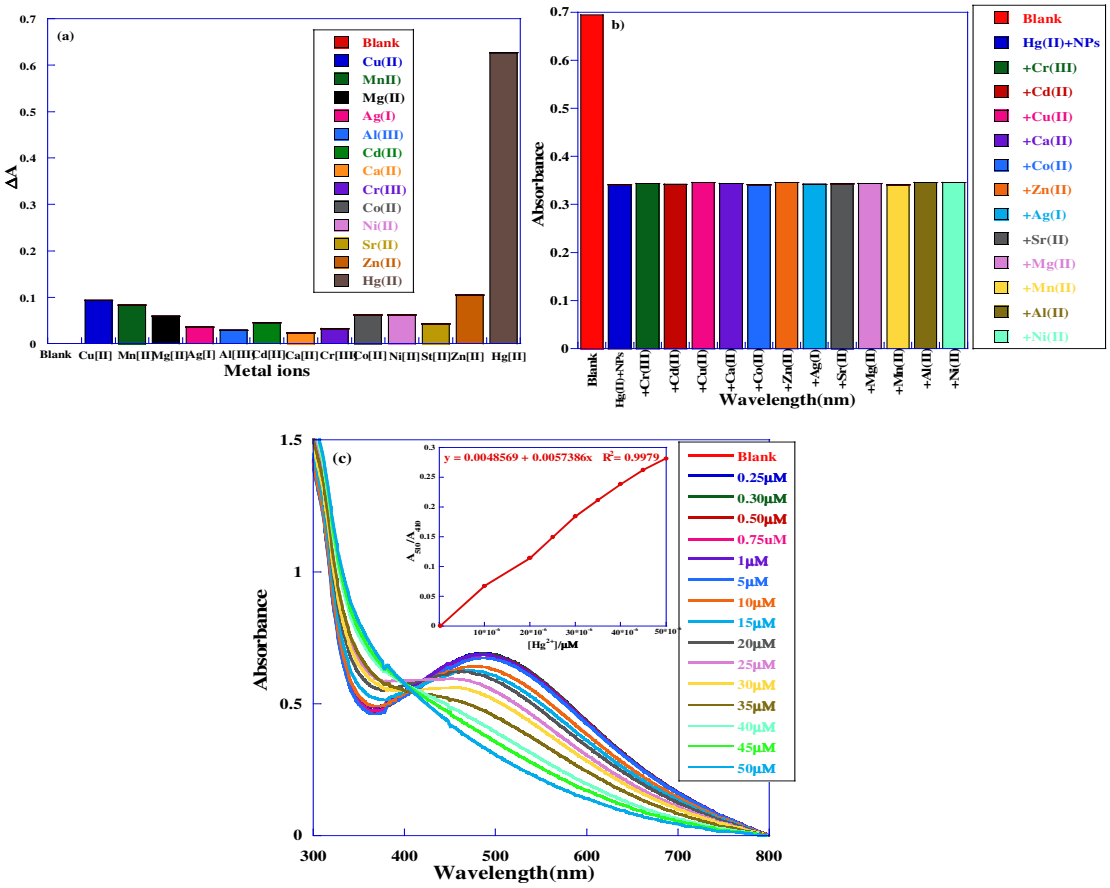

Figure 4(a) The bar graph represent the calorimetric response of PL-CT-AgNPs with various metal ions in terms of change in absorbance ΔA with respect to the blank i.e PL-CT-AgNP (b) The bar graph represent the calorimetric response of PL-CT-AgNPs with mixture of different metal ions in presence of Hg^{2+} in terms of change in absorbance with respect to PL-CT-AgNPs + Hg^{2+} (c) UV-Visible absorbance spectra of PL-CT-AgNPs on addition of [Hg^{2+}] = 0 μM to 50 μM in polluted water sample (inset) Plot of absorption ratio of A_{510}/A_{410} of PL-CT-AgNPs vs. versus concentration of Hg^{2+} in polluted water sample.

Practical Application

The colorimetric response of as synthesized PL-CT-AgNPs towards heavy metal ions is verified in real samples such as in polluted river water. The competency of NPs to detect these metal ions present in the water samples is analyzed by adding different concentrations of Hg^{2+} to the polluted river water sample. A linear decrease in the absorption intensity of PL-CT-AgNPs at 450 nm is detected on varying the concentration of Hg^{2+}from0 μM to 50 μM (Figure 4c). The value of linear regression coefficient (R^2) is obtained to be 0.99790 with the detection limit up to 5 μM (Inset in Figure 4c).

4. Synthesis and Characterization of Gold and Silver nanoparticles in the presence of Gemini Surfactants

The gold nanoparticles (AuNPs) are synthesized by reducing $HAuCl_4$ with $NaBH_4$ in the presence of micelles of gemini surfactants at 70°C. The reactions have been carried out by varying the concentration of surfactants from 1.25mM to 2.5mM to 5mM. Similar reactions are carried out with $AgNO_3$ to synthesize silver nanoparticles (AgNPs) in the presence of micelles of gemini surfactants

in order to compare the results of AgNPs and AuNPs. The Gemini surfactants are 12-2-12 – dimethylene bis(dodecyldimethyl-ammonium bromide), 14-2-14 - dimethylene bis(tetradecyldimethyl-ammonium bromide and 16-2-16 - dimethylene bis(hexadecyldimethyl-ammonium bromide.

Result and Discussion

AuNPs provides a sharp absorbance in the visible region around 520 nm. The shape of resonance peak can be qualitatively related to the nature of NPs. Small and uniform- sized NPs with narrow size distribution give a sharp absorbance, while NPs with wide size distribution or any kind of aggregation show a broad absorbance. The Surface Plasmon Band (SPB) maxima of 12-2-12 stabilized AuNPs at [12-2-12] = 1.25 mM, 2.5 mM and 5 mM are 524nm, 524 nm, and 526 nm, respectively, suggesting that the particle sizes are below 20 nm. These results are supported from TEM, which gives the average particle size of 10 nm. A significant change in absorbance intensity is measured with the change in concentration of [12-2-12]. The intensity increases from [12-2-12] 1.25 mM to 2.5 mM. Further increase in [12-2-12] = 5 mM, intensity decreases. A decrease in intensity suggests the presence of AuNPs in the form of aggregates. Thus, there is deposition of 12-2-12 on the surface of particles, which in turn increases the absorption maxima. However, with an increase in concentration, due to steric effects caused by long chains, the intensity decreases. There is similar increase in SPB maxima from 520 nm to 520 nm to 536 nm at [14-2-14] = 1.25 mM, 2.5 mM and 5mM, respectively. This suggests that average particle size increases with an increase in concentration. However, at [Surfactant] = 5mM, there is significant increase in SPB in 14-2-14 as compared to 12-2-12. As a result, different morphology of particles is obtained such as triangular, hexagon, and pentagon. The intensity increases from [14-2-14] = 1.25 mM to 2.5 mM. Further increase in [14-2-14] = 5 mM, the intensity decreases. There is slight decrease in SPB from 520 nm, 520 nm and 518 nm at [16-2-16] = 1.25 mM, 2.5 mM and 5 mM. TEM results suggest that there are well dispersed gold nanoparticles with size 7 nm. The intensity decreases from 1.25 mM to 2.5 mM. The intensity values are same at 2.5 mM and 5 mM

To quantify the surface adsorption of gemini surfactants on AuNPs surface, FTIR spectral studies of pure 12-2-12, 14-2-14, and 16-2-16 and surfactant capped AuNPs have been carried out. Both spectra are compared. It is well known that the symmetric and antisymmeteric stretching vibrations of methylene can be used as an indicator of ordering of alkyl chains and higher energies of stretching vibrations corresponds to more gauche defects. The symmetric and asymmetric stretching vibrations of methylene of pure 16-2-16 are located at 2851 cm^{-1} and 2919 cm^{-1}, and those of 16-2-16 capped AuNPs are located at 2855 cm^{-1} and 2924 cm^{-1}. The slight shift to higher frequencies indicates that the methylene chain changes from more ordered, predominantly trans conformation in the solid phase to a more disordered structure which corresponds to small increase of the number of gauche defects. The intensities of $C\text{-}N^{+}$ stretching bands of 16-2-16 molecules coated on AuNPs at 924 cm^{-1} and 957cm^{-1} disappeared and a new peak at 1019 cm^{-1} is formed, suggesting that 16-2-16 head groups are directed at AuNPs surface. Similar behaviors demonstrated in 12-2-12 and 14-2-14. Apart from this, the peak at 721 cm^{-1} in pure 12-2-12/14-2-14/16-2-16 arises from the rocking mode of the methylene $(\text{-CH2-})_n$ chain, which shifts to higher frequencies for both 12-2-12 and 14-2-14 as compared to 16-2-16, indicating the presence of much ordered arrangement of surfactant hydrophobic tails on Au surface in the form of surfactant capping film. The particle sizes are decreasing with the increase in concentration. A significant change in absorbance intensity is measured with the change in concentration of [12-2-12]. The intensity decreases from [12-2-12] = 1.25 mM to 2.5 mM to 5.0 mM. Similar behavior is observed in the case of 14-2-14 and 16-2-16 capped AgNPs, where particle size decreases as SPB shifts to lower wavelength region. The intensity decreases from 1.25 mM to 2.5 mM and then increases from 2.5 mM to 5mM in 14-2-14 capped AgNPs, however intensity decreases in 16-2-16 as concentration increases. The results are supported from TEM analysis.

(a) **(b)**

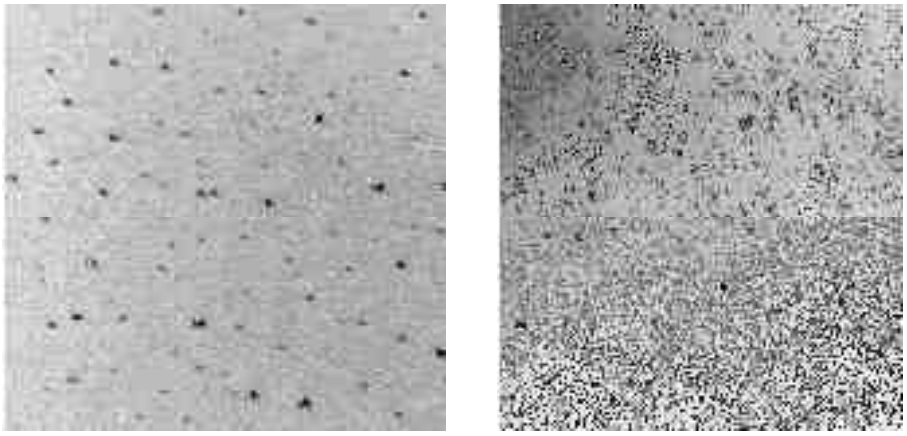

Figure 1: TEM images of (a) 12-2-12 and (b) 14-2-14.